Stem Cell Reports, Volume *16*

Supplemental Information

Defective autophagy and increased apoptosis contribute toward the pathogenesis of FKRP-associated muscular dystrophies

Carolina Ortiz-Cordero, Claudia Bincoletto, Neha R. Dhoke, Sridhar Selvaraj, Alessandro Magli, Haowen Zhou, Do-Hyung Kim, Anne G. Bang, and Rita C.R. Perlingeiro

Figure S1

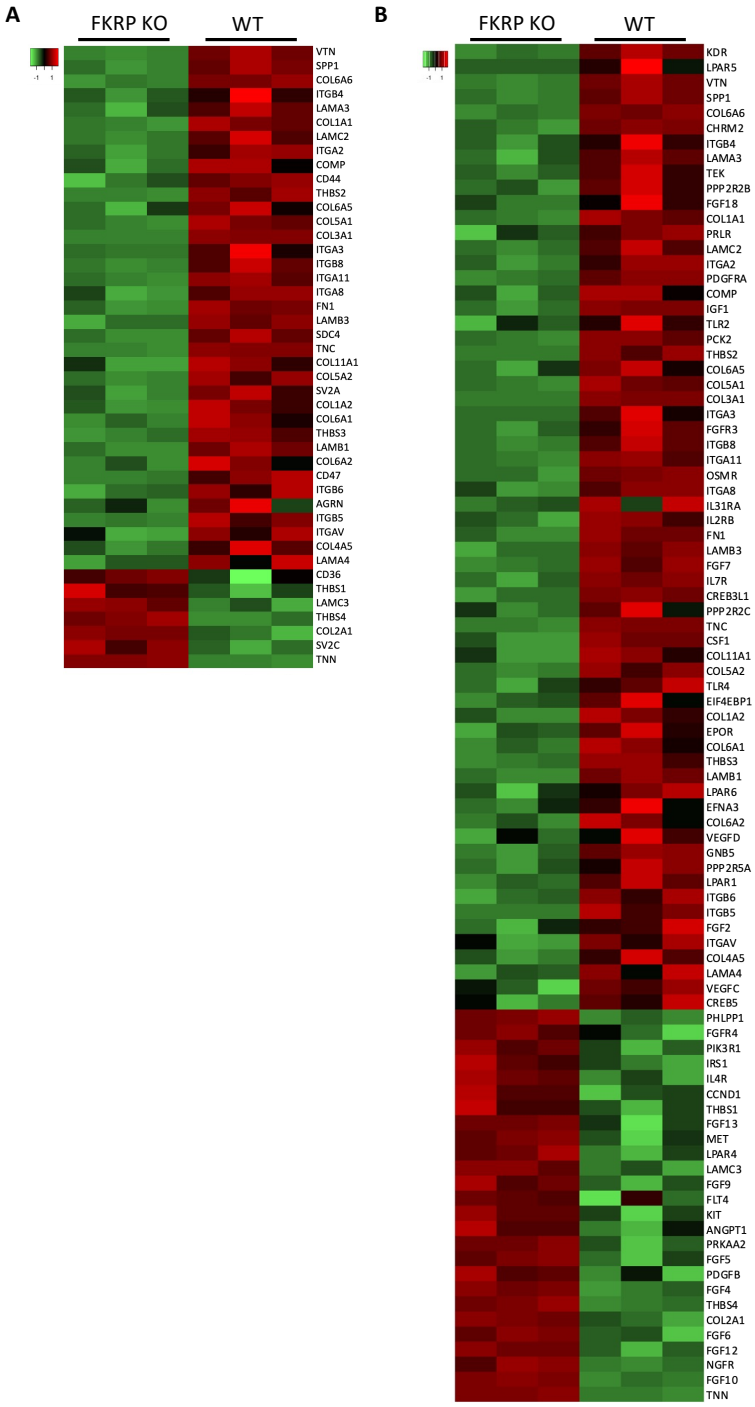
A
FKRP KO
WT
VTN
SPP1
COL6A6
ITGB4
LAMA3
COL1A1
LAMC2
ITGA2
COMP
CD44
THBS2
COL6A5
COL5A1
COL3A1
ITGA3
ITGB8
ITGA11
ITGA8
FN1
LAMB3
SDC4
TNC
COL11A1
COL5A2
SV2A
COL1A2
COL6A1
THBS3
LAMB1
COL6A2
CD47
ITGB6
AGRN
ITGB5
ITGAV
COL4A5
LAMA4
CD36
THBS1
LAMC3
THBS4
COL2A1
SV2C
TNN
B
FKRP KO
WT
KDR
LPAR5
VTN
SPP1
COL6A6
CHRM2
ITGB4
LAMA3
TEK
PPP2R2B
FGF18
COL1A1
PRLR
LAMC2
ITGA2
PDGFRA
COMP
IGF1
TLR2
PCK2
THBS2
COL6A5
COL5A1
COL3A1
ITGA3
FGFR3
ITGB8
ITGA11
OSMR
ITGA8
IL31RA
IL2RB
FN1
LAMB3
FGF7
IL7R
CREB3L1
PPP2R2C
TNC
CSF1
COL11A1
COL5A2
TLR4
EIF4EBP1
COL1A2
EPOR
COL6A1
THBS3
LAMB1
LPAR6
EFNA3
COL6A2
VEGFD
GNB5
PPP2R5A
LPAR1
ITGB6
ITGB5
FGF2
ITGAV
COL4A5
LAMA4
VEGFC
CREB5
PHLPP1
FGFR4
PIK3R1
IRS1
IL4R
CCND1
THBS1
FGF13
MET
LPAR4
LAMC3
FGF9
FLT4
KIT
ANGPT1
PRKAA2
FGF5
PDGFB
FGF4
THBS4
COL2A1
FGF6
FGF12
NGFR
FGF10
TNN

Figure S2

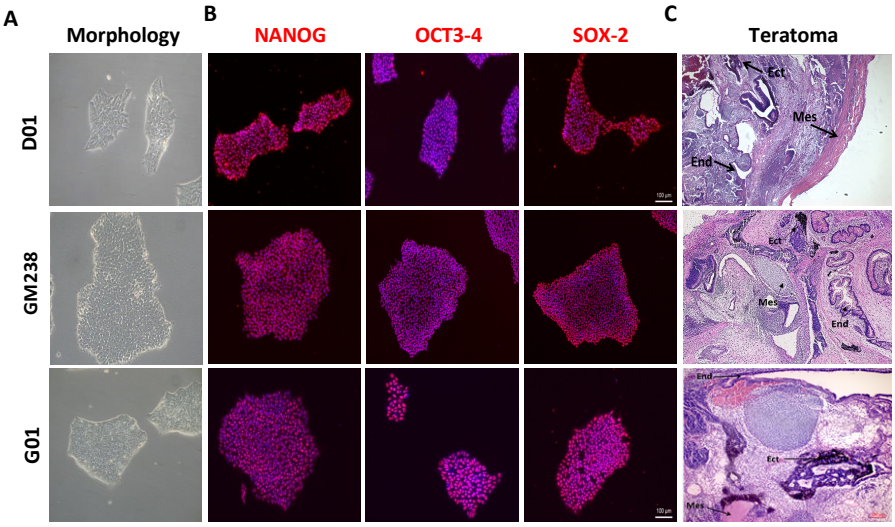
A
Morphology
B
NANOG
OCT3-4
SOX-2
C
Teratoma
D01
GM238
G01
Ect
Mes
End

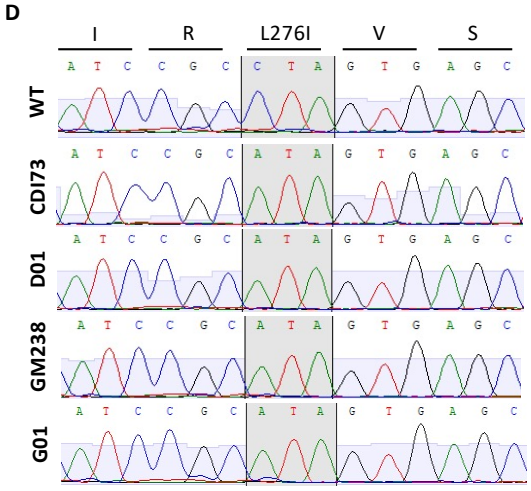
D
I
R
L276I
V
S
WT
CDI73
D01
GM238
G01

Figure S3

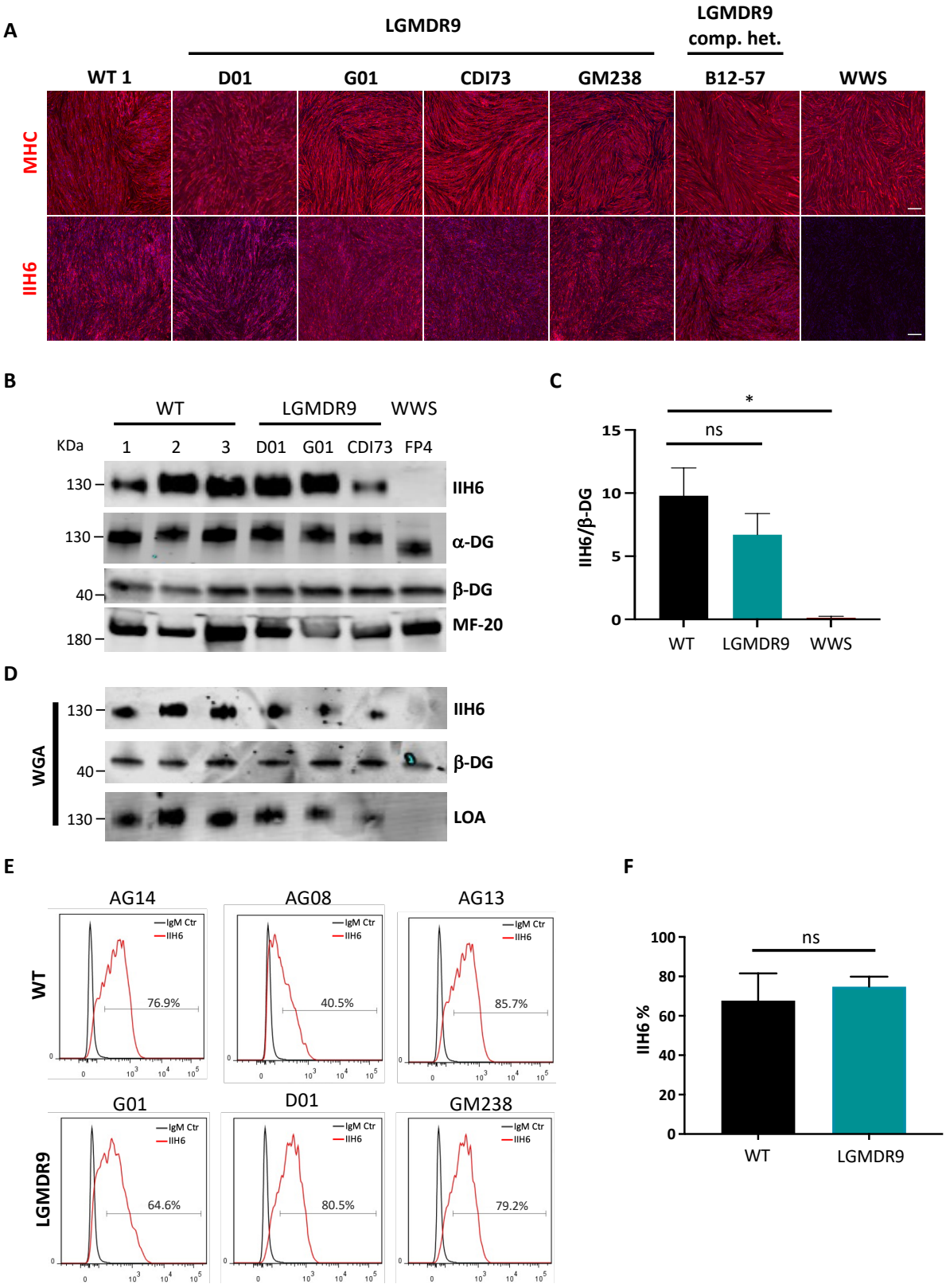
A
LGMDR9
LGMDR9 comp. het.
WT 1
D01
G01
CDI73
GM238
B12-57
WWS
MHC
IIH6
B
WT
LGMDR9
WWS
KDa
1
2
3
D01
G01
CDI73
FP4
130
IIH6
130
α-DG
40
β-DG
180
MF-20
C
*
ns
15
10
5
0
IIH6/β-DG
WT
LGMDR9
WWS
D
WGA
130
IIH6
40
β-DG
130
LOA
E
AG14
AG08
AG13
WT
IgM Ctr
IIH6
76.9%
40.5%
85.7%
G01
D01
GM238
LGMDR9
64.6%
80.5%
79.2%
F
ns
100
80
60
40
20
0
IIH6 %
WT
LGMDR9

Figure S4

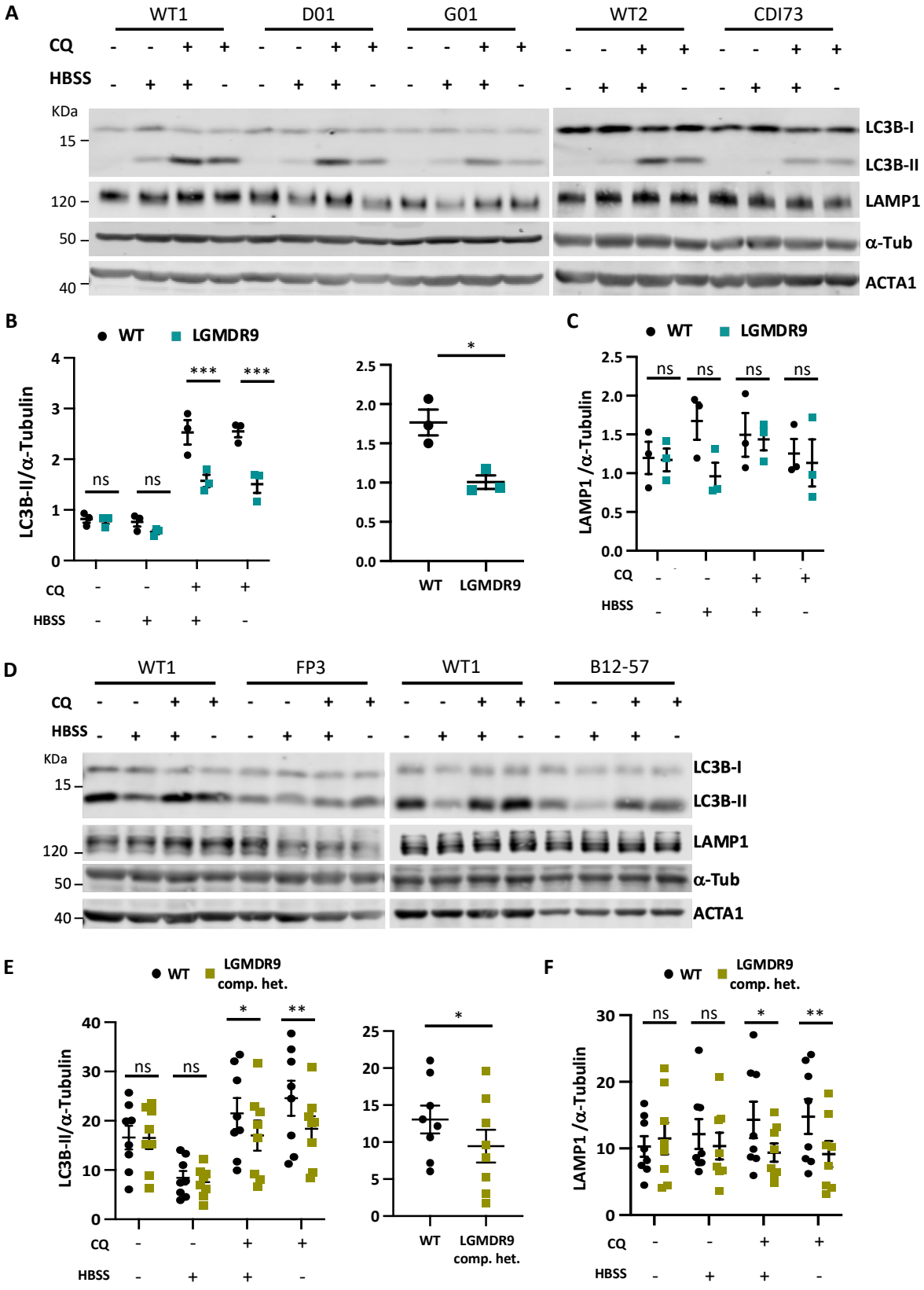
A
WT1
D01
G01
WT2
CDI73
CQ
HBSS
KDa
15
120
50
40
LC3B-I
LC3B-II
LAMP1
α-Tub
ACTA1
B
WT
LGMDR9
LC3B-II/α-Tubulin
ns
***
*
C
LAMP1 /α-Tubulin
D
FP3
B12-57
E
LGMDR9 comp. het.
**
F

Figure S5

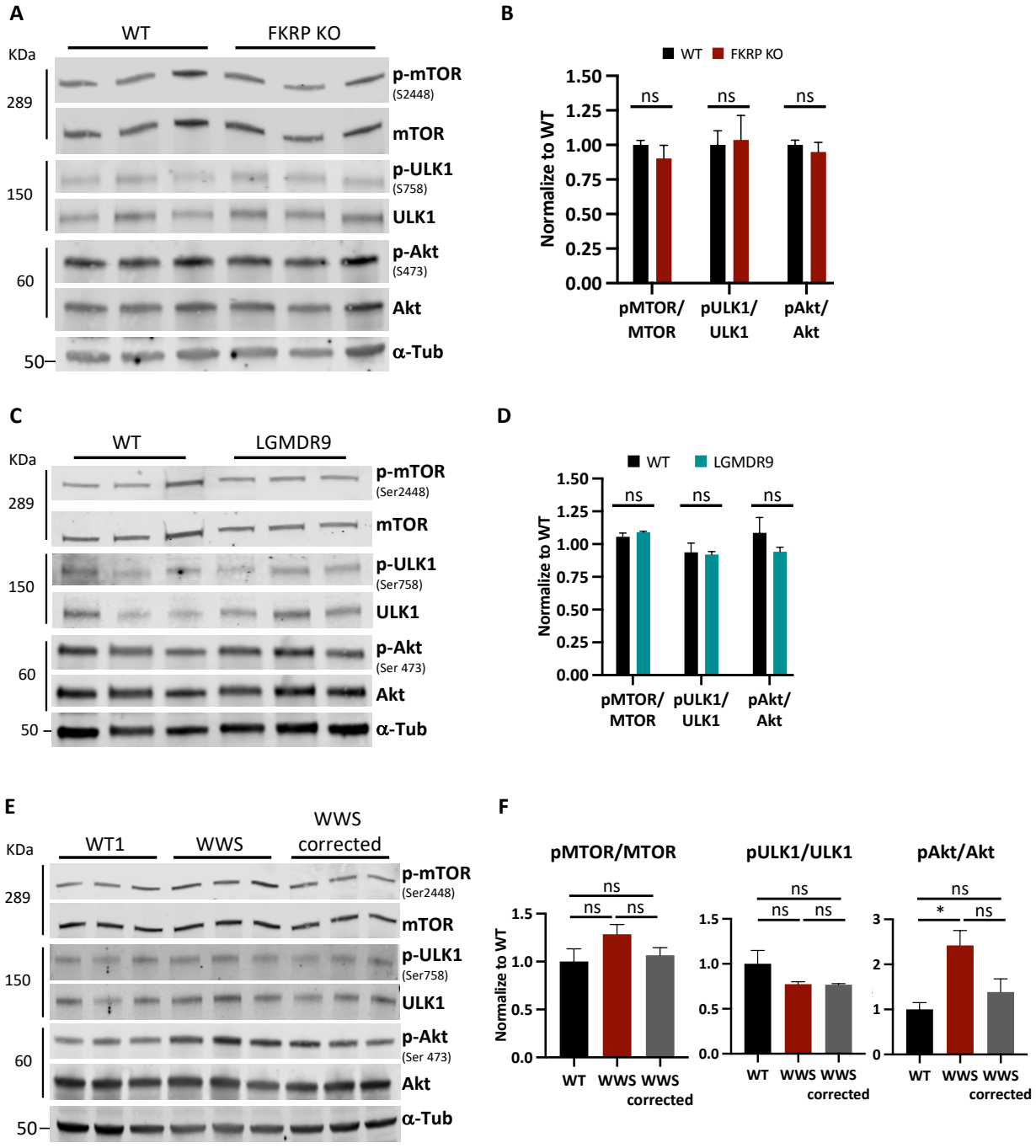
A
WT
FKRP KO
KDa
289
150
60
50
p-mTOR
(S2448)
mTOR
p-ULK1
(S758)
ULK1
p-Akt
(S473)
Akt
α-Tub
B
WT
FKRP KO
Normalize to WT
1.50
1.25
1.00
0.75
0.50
0.25
0.00
ns
pMTOR/
MTOR
pULK1/
ULK1
pAkt/
Akt
C
WT
LGMDR9
KDa
289
150
60
50
p-mTOR
(Ser2448)
mTOR
p-ULK1
(Ser758)
ULK1
p-Akt
(Ser 473)
Akt
α-Tub
D
WT
LGMDR9
Normalize to WT
1.50
1.25
1.00
0.75
0.50
0.25
0.00
ns
pMTOR/
MTOR
pULK1/
ULK1
pAkt/
Akt
E
KDa
WT1
WWS
WWS
corrected
289
150
60
50
p-mTOR
(Ser2448)
mTOR
p-ULK1
(Ser758)
ULK1
p-Akt
(Ser 473)
Akt
α-Tub
F
pMTOR/MTOR
pULK1/ULK1
pAkt/Akt
Normalize to WT
1.5
1.0
0.5
0.0
3
2
1
0
ns
*
WT
WWS
WWS
corrected

Figure S6

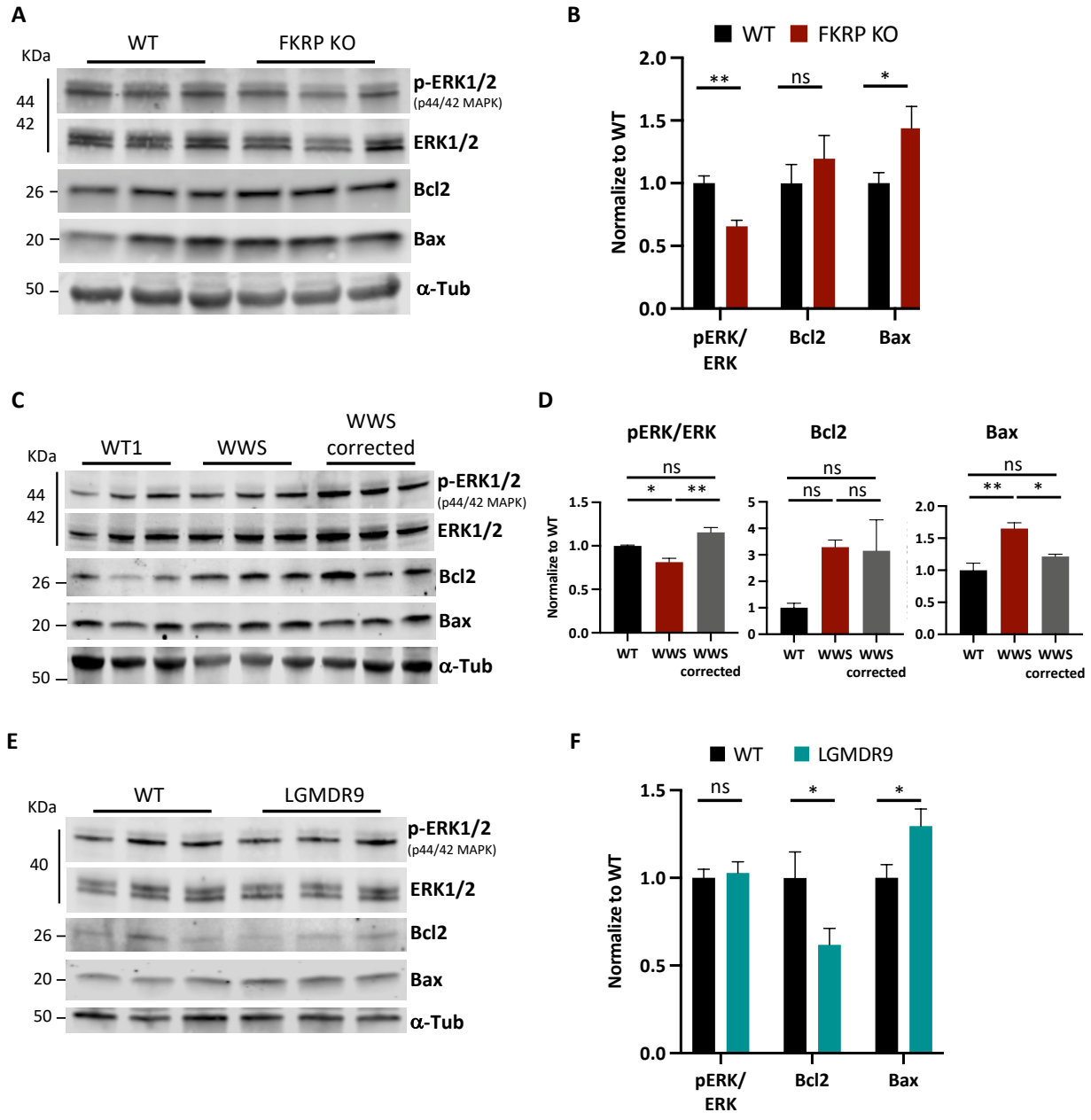
A
KDa
WT
FKRP KO
44
42
p-ERK1/2
(p44/42 MAPK)
ERK1/2
26
Bcl2
20
Bax
50
α-Tub
B
WT
FKRP KO
Normalize to WT
2.0
1.5
1.0
0.5
0.0
**
ns
*
pERK/
ERK
Bcl2
Bax
C
KDa
WT1
WWS
WWS
corrected
44
42
p-ERK1/2
(p44/42 MAPK)
ERK1/2
26
Bcl2
20
Bax
50
α-Tub
D
pERK/ERK
Bcl2
Bax
Normalize to WT
ns
*
**
WT
WWS
WWS
corrected
E
KDa
WT
LGMDR9
40
p-ERK1/2
(p44/42 MAPK)
ERK1/2
26
Bcl2
20
Bax
50
α-Tub
F
WT
LGMDR9
Normalize to WT
1.5
1.0
0.5
0.0
ns
*
pERK/
ERK
Bcl2
Bax

Figure S1. Differentially expressed genes in FKRP KO myotubes and isogenic WT.

(A-C) Heatmap of differentially expressed genes associated with (A) calcium signaling pathway, (B) extracellular matrix receptor (ECM) interaction, and (C) PI3K-Akt signaling pathway in isogenic WT and FKRP KO myotubes.

Figure S2. Characterization of LGMDR9 FKRP patient specific-iPS cells.

(A-B) Representative images show typical (A) pluripotent colony morphology, (B) immunostaining for OCT3/4, SOX2, and NANOG (red) for D01, GM283, and G01 iPS cells. DAPI stains nuclei in blue.

(C) Representative image shows hematoxylin-eosin staining of a teratoma denoting the presence of tissues derived from all three germ layers for D01, GM283, and G01 iPS cells.

(D) Sequencing chromatograms show CDI73, D01, GM283, and G01 iPS cell lines are homozygous for FKRP mutation c.826C>A. Unaffected iPS cells were used as a control for given sequences.

Figure S3. Characterization of α-dystroglycan glycosylation in FRKP mutant cells.

(A) Representative immunostaining for MHC and IIH6 (red) for LGMDR9 D01, G01, CDI73, and GM238, LGMDR9 compound heterozygous (comp. het.) B12-57, WWS, and WT iPS cell-derived myotubes DAPI stained nuclei (in blue). Scale bar, 200µm.

(B) Western blot for IIH6 in WT1, WT2 WT3, LGMDR9 D01, G01 CDI73, and WWS myotubes. β-DG was used as the loading control.

(C) Graph bars show respective quantification of IIH6 (B) normalized to β-DG. *$p<0.05$ by one-way ANOVA followed by Sidak's multiple comparison test. Error bars represent standard errors of 3 independent experiments.

(D) Representative WGA pull-down laminin overlay assay (LOA) for samples in (B).

(E) Histogram of flow cytometry analysis for IIH6 in LGMDR9 and WT control fibroblasts.

(F) Bar graph shows quantification of (E). Significance was evaluated by unpaired Student's t-test. Error bars represent standard errors of 3 independent cell lines.

Figure S4. Autophagy is decreased in LGMDR9 myotubes.

(A) Western blot for LC3B-II and LAMP1 in WT1, WT2, and LGMDR9 D01, G01, CDI73 myotubes. Cells were assessed under basal or Hanks' Balanced Salt Solution (HBSS), with or without 100 μM chloroquine (CQ).

(B-C) Respective quantification for LC3B-II (B) and LAMP1 (C) of western blots shown in (A) normalized to α-tubulin. Right panel in (B) shows flux calculated as the difference in LC3B-II levels of HBSS-treated myotubes with and without CQ. *p<0.05, ***p<0.001, by RM two-way ANOVA followed by Sidak's multiple comparison test and paired Student's t-test in (B) right panel. Each symbol represents the average of 4-5 repetitions for each cell line. Error bars are mean ± SEM.

(D) Western blot for LC3B-II and LAMP1 in WT1, and LGMDR9 compound heterozygous (comp. het.) FP3 and B12-57 myotubes. Cells were assessed under basal or Hanks' Balanced Salt Solution (HBSS), with or without 100 μM chloroquine (CQ).

(E-F) Respective quantification for LC3B-II (E) and LAMP1 (F) of western blots shown in (D) normalized to α-tubulin. Right panel in (E) shows flux calculated as the difference in LC3B-II levels of HBSS-treated myotubes with and without CQ. *p<0.05, **p<0.01, by RM two-way ANOVA followed by Sidak's multiple comparison test and paired Student's t-test in (E) right panel. Error bars are mean ± SEM for 8 independent experiments, 4 independent experiments for each LGMDR9 comp. het. cell line. Error bars are mean ± SEM.

Figure S5. Akt and mTOR activity in FKRP KO and patient-derived myotubes

(A) Western blot for mTOR, ULK1, and Akt activity in FKRP KO and parental WT myotubes. α-tubulin was used as loading controls.

(B) Bar graphs show respective quantification of (A) normalized to parental WT. ns p>0.05 by unpaired Student's t-test. Error bars represent standard errors of 3 independent experiments.

(C) Western blot for mTOR, ULK1, and Akt activity in D01, G01, CDI73 LGMDR9 myotubes and WT1, WT3, and WT3 controls. α-tubulin was used as loading controls.

(D) Bar graphs show respective quantification of (C) normalized to isogenic WT. ns p>0.05 by unpaired Student's t-test. Error bars represent standard errors of 3 independent experiments.

(E) Western blot for mTOR, ULK1, and Akt activity in WT1, WWS, and WWS corrected iPS cell-derived myotubes. α-tubulin was used as loading controls.

(F) Bar graphs show respective quantification of (E) normalized to WT. *p<0.05 by one-way ANOVA followed by Sidak's multiple comparison test. Error bars represent standard errors of 3 independent experiments.

Figure S6. ERK1/2 activity and markers of apoptosis in FKRP KO and patient-derived myotubes

(A) Western blot for phospho-ERK1/2, ERK1/2, Bax, and Bcl2 in FKRP KO myotubes and WT control. α-tubulin was used as loading controls.

(B) Quantification of (A) normalized to WT counterpart. *p<0.05, **p<0.01 by unpaired Student's t-test. Error bars represent standard errors of 3 independent experiments.

(C) Western blot for ERK1/2 activity, Bcl-2, and Bax in WT1, WWS, and WWS corrected myotubes. α-tubulin was used as loading controls.

(D) Quantification of (C) normalized to WT. *p<0.05, **p<0.01 by one-way ANOVA followed by Sidak's multiple comparison test. Error bars represent standard errors of 3 independent experiments.

(E) Western blot for ERK1/2 activity, Bcl-2 and Bax in WT1, WT2, and WT3 controls and D01, G01, CDI73 LGMDR9 myotubes. α-tubulin was used as loading controls.

(F) Quantification of (E) normalized to WT. *p<0.05. by unpaired Student's t-test. Error bars represent standard errors of 3 independent experiments for 3 LGMDR9 and 3 WT lines.

Table S1. Pluripotent stem cell lines and fibroblast used in this study.

Cell line	Cell type	Clinical Phenotype	Age at biopsy	Nucleotide variant	Amino Acid	Reference
WT (H9)	ESC	none	-	-	-	WiCell
WT1 (PLZ)	iPSC	none	Adult	-	-	(Darabi et al., 2012)
WT3 (TC1133)	iPSC	none	Adult	-	-	(Selvaraj et al., 2019)
WT3 (B05)	iPSC	none	Adult	-	-	(Darabi *et al.*, 2012)
AG08	Fibroblast	none	31	-	-	Coriell Institute
AG13	Fibroblast	none	30	-	-	Coriell Institute
AG14	Fibroblast	none	35	-	-	Coriell Institute
CDI73	iPSC	LGMDR9	Adult	c.826C>A c.826C>A	p.Leu276Ile p.Leu276Ile	Cellular Dynamics
GM238	Fibroblast iPSC	LGMDR9	38	c.826C>A c.826C>A	p.Leu276Ile p.Leu276Ile	This study
D01	Fibroblast iPSC	LGMDR9	27	c.826C>A c.826C>A	p.Leu276Ile p.Leu276Ile	This study
G01	Fibroblast iPSC	LGMDR9	8	c.826C>A c.826C>A	p.Leu276Ile p.Leu276Ile	This study
B12-57	iPSC	LGMDR9	3	c.826C>A c.534G>T	p.Leu276Ile p.Trp178Cys	(Nickolls et al., 2020)
FP3	iPSC	LGMDR9/ CMD	1.25	c.217C>T c.826C>A	p.Glu73 OCH p.Leu276Ile	(Dhoke et al., 2021)
FP4	iPSC	WWS	< 1yr	c.558dupC c.1418T>G	p.Ala187Fs p.Phe473Cys	(Ortiz-Cordero et al., 2021)

Table S2. Muscle biopsies used in this study

Identifier	Sex	Clinical Phenotype	Age at biopsy	Nucleotide variant	Amino Acid
CTRL5a	F	none	9	-	-
CTRL6b	M	none	3	-	-
CTRL61	F	none	34	-	-
04-07071	F	CMD	1	c.1387A>G c.1387A>G	p.Asn463Asp p.Asn463Asp
10-11175	M	CMD	2	c.1387A>G c.1387A>G	p.Asn463Asp p.Asn463Asp
17-39292	M	CMD	2	c.1387A>G c.1387A>G	p.Asn463Asp p.Asn463Asp
07-17608	F	LGMDR9	34	c.826C>A c.826C>A	p.Leu276Ile p.Leu276Ile
12-18979	M	LGMDR9	7	c.826C>A c.826C>A	p.Leu276Ile p.Leu276Ile
12-22942	M	LGMDR9	28	c.826C>A c.826C>A	p.Leu276Ile p.Leu276Ile

Table S3. Antibodies used throughout this study

Target	Company/Source	Concentration	Catalog No.
α-Dystroglycan	Millipore Sigma Developmental Studies Hybridoma Bank	1:1000 (WB) 1:50 (IF)	05-593 IIH6 C4
α-Tubulin (TU-02)	Santa Cruz Biotechnology	1:1000	sc-8035
β-Dystroglycan (concentrated)	Developmental Studies Hybridoma Bank	1:1500	MANDAG2 (7D11)
Actin (α-Sarcomeric)	Sigma-Aldrich	1:1000	A2172
Akt	Cell Signaling Technologies	1:1000	9272
Bax	Proteintech	1:2000	50599-2-Ig
Bcl-2	Proteintech	1:1000	12789-1-AP
Dystroglycan	R&D Systems	1:1000	AF6868
Laminin	Sigma-Aldrich	1:1000	L9393
LAMP1	Abcam	1:1000	ab24170
LC3B	Novus Biologicals Cell Signaling Technologies	1:1000 (WB) 1:250 (IF)	NB100-2220 2775
mTOR (7C10)	Cell Signaling Technologies	1:1000	2983
Myosin heavy chain	Developmental Studies Hybridoma Bank	1:200 (WB) 1:50 (IF)	MF-20
p44/42 MAPK (Erk1/2) (Thr202/Tyr204)	Cell Signaling Technologies	1:1000	9102
Phospho-Akt (Ser473) (D9E)	Cell Signaling Technologies	1:1000	4060
Phospho-mTOR (Ser2448) (D9C2)	Cell Signaling Technologies	1:1000	5536
Phospho-p44/42 MAPK (Erk1/2) (Thr202/Tyr204)	Cell Signaling Technologies	1:1000	4370
Phospho-ULK1 (Ser757)	Cell Signaling Technologies	1:1000	6888
ULK1 (D8H5)	Cell Signaling Technologies	1:1000	8054

Supplemental references

Darabi, R., Arpke, R.W., Irion, S., Dimos, J.T., Grskovic, M., Kyba, M., and Perlingeiro, R.C. (2012). Human ES- and iPS-derived myogenic progenitors restore DYSTROPHIN and improve contractility upon transplantation in dystrophic mice. Cell Stem Cell *10*, 610-619. 10.1016/j.stem.2012.02.015.
Dhoke, N.R., Kim, H., Selvaraj, S., Azzag, K., Zhou, H., Oliveira, N.A.J., Tungtur, S., Ortiz-Cordero, C., Kiley, J., Lu, Q.L., et al. (2021). A universal gene correction approach for FKRP-associated dystroglycanopathies to enable autologous cell therapy. Cell Reports *36*. 10.1016/j.celrep.2021.109360.
Nickolls, A.R., Lee, M.M., Zukosky, K., Mallon, B.S., and Bonnemann, C.G. (2020). Human embryoid bodies as a 3D tissue model of the extracellular matrix and alpha-dystroglycanopathies. Dis Model Mech, dmm042986. 10.1242/dmm.042986.
Ortiz-Cordero, C., Magli, A., Dhoke, N.R., Kuebler, T., Selvaraj, S., Oliveira, N.A., Zhou, H., Sham, Y.Y., Bang, A.G., and Perlingeiro, R.C. (2021). NAD+ enhances ribitol and ribose rescue of alpha-dystroglycan functional glycosylation in human FKRP-mutant myotubes. Elife *10*. 10.7554/eLife.65443.
Selvaraj, S., Mondragon-Gonzalez, R., Xu, B., Magli, A., Kim, H., Laine, J., Kiley, J., McKee, H., Rinaldi, F., Aho, J., et al. (2019). Screening identifies small molecules that enhance the maturation of human pluripotent stem cell-derived myotubes. Elife *8*. 10.7554/eLife.47970.